Table S1 – Comparison of CypA observed Bragg data vs. calculated from Normal Modes.

Resolution (Å)	R-factor	CC
44.560-11.070	0.5713	0.4144
11.070-8.698	0.3325	0.6957
8.697-6.834	0.2987	0.7324
6.831-5.369	0.2944	0.788
5.366-4.217	0.2556	0.8362
4.216-3.314	0.2592	0.8153
3.312-2.603	0.3092	0.7586
2.602-2.045	0.3355	0.6972
2.045-1.606	0.3602	0.6928
1.606-1.262	0.41	0.5964
1.262-1.200	0.4509	0.3817
All	0.3869	0.855

Table S2 - Comparison of Trypsin observed Bragg data vs. calculated from Normal Modes.

Resolution (Å)	R-factor	CC
26.837-10.849	0.511	0.4285
10.837-8.689	0.3368	0.7372
8.678-6.955	0.3786	0.6475
6.937-5.569	0.3312	0.7195
5.564-4.457	0.2509	0.8368
4.455-3.569	0.2322	0.8663
3.568-2.857	0.2684	0.8155
2.857-2.288	0.2924	0.761
2.288-1.832	0.2911	0.7678
1.832-1.467	0.3072	0.7564
1.467-1.200	0.3271	0.7048
All	0.3106	0.887

Table S3. Refinement statistics for CypA and trypsin models, before TLS modeling is applied.

	CypA	**Trypsin**
Resolution range, Å	38.66-1.4	23.29-1.25
Space group	P 21 21 21	P 21 21 21
Unit cell, Å	42.91, 52.44, 89.12	54.81, 58.51, 67.42
Completeness (%)	98	95
R_{work} (%)	17.88	15.9
R_{free} (%)	19.5	17.41
RMS (bonds, Å)	0.007	0.013
RMS (angles, degrees)	1.16	1.61
Ramachandran favored %	97	98
Ramachandran allowed %	3	2
Ramachandran outliers %	0	0
Clashscore	0.79	2.59
Average B-factor, $Å^2$	21.42	14.57

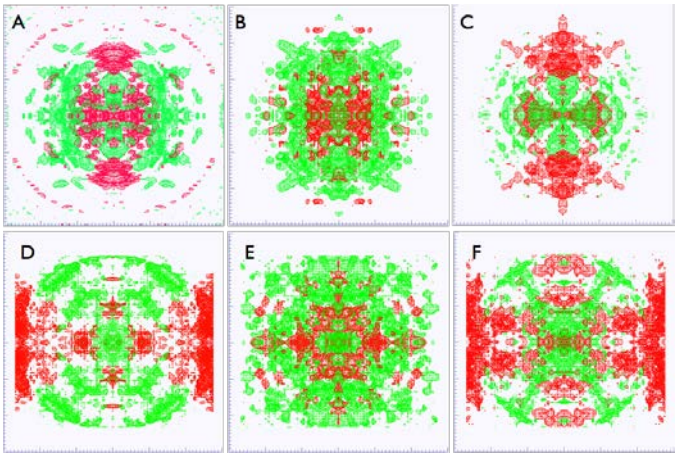

Figure S1. Visualization of anisotropic diffuse intensities. (A) Symmetrized CypA experimental data with isosurfaces shown using wireframes at a level of 2 photon counts in the resolution range 4.16 Å – 2.97 Å. Positive intensity is rendered in green, negative in red. (B) Isosurfaces for diffuse scattering predicted by the CypA LLM model. (C) Residual diffuse scattering (experimental data (A) minus LLM (B)). (D) Symmetrized Trypsin experimental data with isosurfaces shown using wireframes at a level of 3 photon counts in the resolution range 4.53 Å – 3.26. (E) Isosurfaces for diffuse scattering predicted by the Trypsin LLM model. (F) Residual diffuse scattering (experimental data (D) minus LLM (E)).

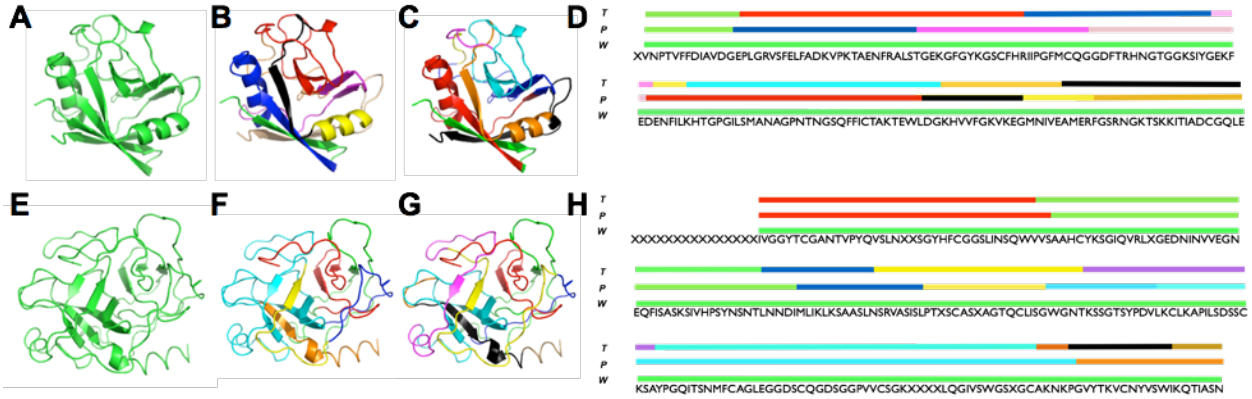

Figure S2. Rigid body domain definitions used for TLS models. CypA and Trypsin TLS groups shown on the tertiary structure for whole molecule (A, E), Phenix (B, F), and TLSMD (C, G) and shown on the primary sequence (D, H).

Figure S3: Simulated diffraction images for trypsin frame 45 obtained using: (A) liquid-like motions model; (B) integrated 3D diffuse data; (C) elastic network model.

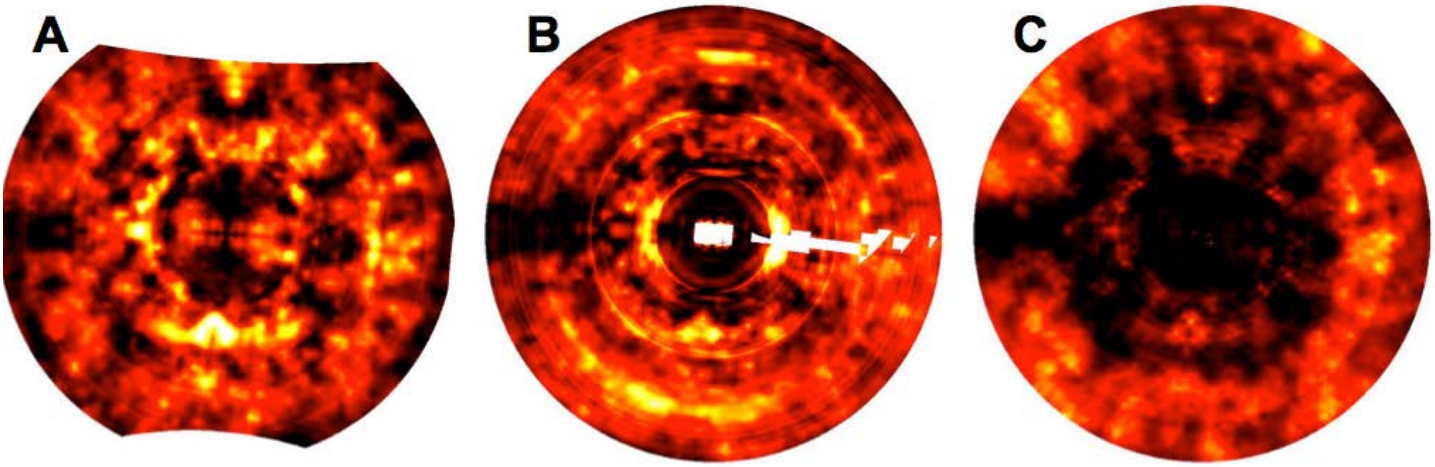

Figure S4: Normal modes models for a) CypA and b) Trypsin. The RCSB deposited structure is shown in blue with thicker ribbon. Every 5th ensemble member of the 50 member ensemble is shown in a different color. Displacements along the top 10 modes are shown with the sum of squares of displacements equal to 1 Å.

A

B

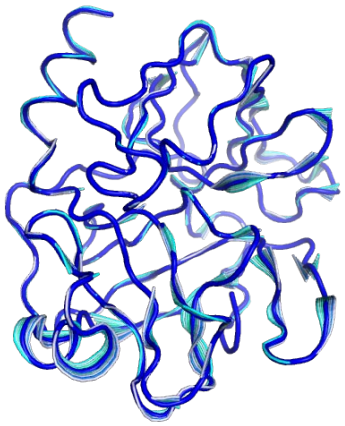

Figure S5: Simulation of CypA diffraction images using integrated 3D data. Left: raw processed frame 67, after the mode filter step (Methods). Middle: isosurface in anisotropic diffuse intensity at a level of 2 photons, displayed using ParaView (http://www.paraview.org/). Right: Simulated diffuse intensity for frame 67 computed using 3D diffuse intensity. For each image, the minimum value within each pixel-width ring about origin has been subtracted from each pixel value, to enhance the visualization of anisotropic diffuse features. Images are displayed using a heat map in Adxv.

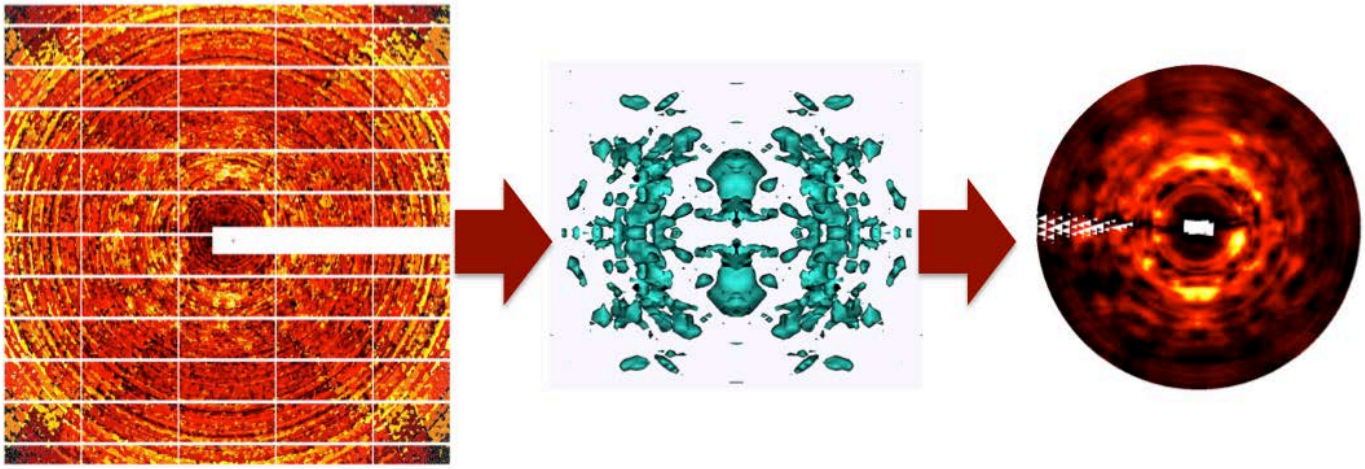

Figure S6: Simulation of trypsin diffraction images using integrated 3D data. Left: raw processed frame 45, after the mode filter step (Methods). Middle: isosurface in anisotropic diffuse intensity at a level of 3 photons, displayed using ParaView (http://www.paraview.org/). Right: Simulated diffuse intensity for frame 45 computed using 3D diffuse intensity. Images were processed and displayed as in Fig. S6.

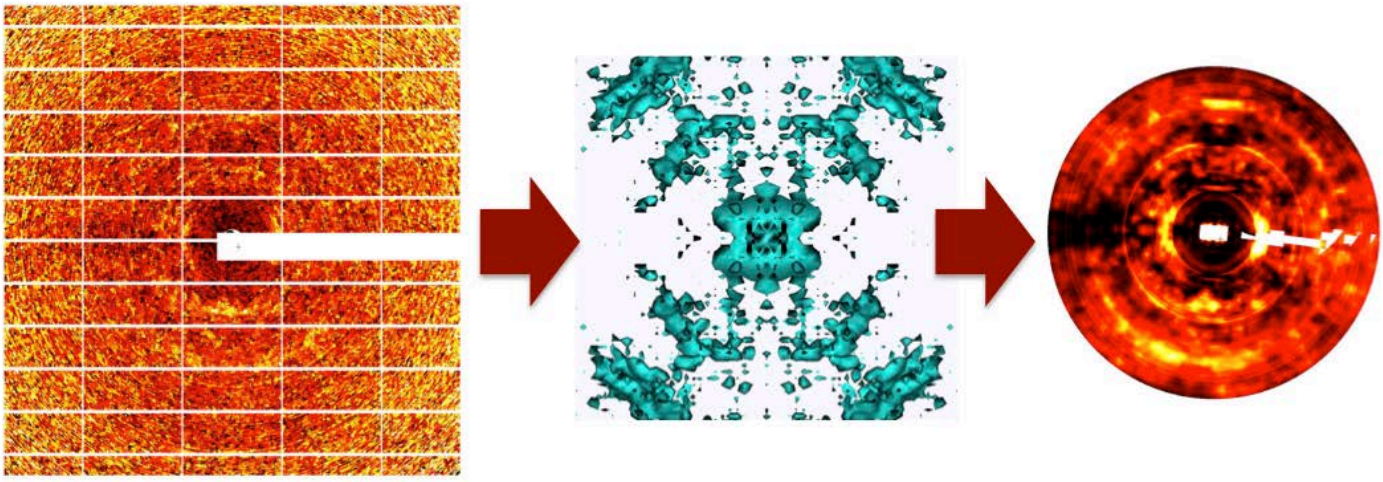

Supplementary Text

Methods

Protein purification and crystallization

Trypsin crystals were obtained according to the method of Liebschner *et.al* (1). Lyophilized bovine pancreas trypsin was purchased from Sigma-Aldrich (T1005) and dissolved at a concentration of 30 mg/mL into 30mM HEPES pH 7.0, 5 mg/mL benzamidine and 3mM $CaCl_2$. Crystals were obtained from a solution of 200mM Ammonium sulfate, 100mM Na cacodylate pH 6.5, 20% PEG 8000 and 15% glycerol. CypA was purified and crystallized as previously described (2). Briefly, the protein was concentrated to 60 mg/mL in 20mM HEPES pH 7.5, 100mM NaCl and 500mM TCEP. Trays were set with a precipitant solution of 100mM HEPES pH 7.5, 22% PEG 3350 and 5mM TCEP. Both crystal forms were obtained using the hanging-drop method.

Crystallographic data collection

Diffraction data were collected on beamline 11-1 at the Stanford Synchrotron Radiation Lightsource (Menlo Park, CA). X-ray diffraction images were obtained using a Dectris PILATUS 6M Pixel Array Detector (PAD). Each dataset was collected from a single crystal at an ambient temperature of 273K. To prevent dehydration, crystals were coated in a thin film of paratone with minimal surrounding mother liquor. For CypA, a single set of 0.5 degree oscillation images were collected and used for both Bragg and diffuse data processing. A total of 360 images were collected across a 180 degree phi rotation. The Trypsin diffraction data consisted of one degree oscillations across a 135 degree phi rotation; this dataset was similarly used for both Bragg and diffuse data analysis. Both datasets were collected to optimize the Bragg signal, not the diffuse signal. Although not used here, we note that data collection using a PAD with fine phi slicing should be especially well suited for simultaneous collection of Bragg and diffuse data, as it would enable integration of diffuse intensity at a tunable level of detail in reciprocal space.

Bragg data processing

Bragg diffraction data were processed using XDS and XSCALE (3) within the *xia2* software package (4). Molecular replacement solutions were found using Phaser (5) within the *Phenix* software suite (6). The PDB search models were 4I8G for trypsin, and 2CPL for CypA. Initial structural refinement was performed using *phenix.refine* (7). The strategy included refinement of individual atomic coordinates and water picking. Both the X-ray/atomic displacement parameters and X-ray/stereochemistry weights were optimized. Isotropic B-factors were chosen for the initial structures to allow for non-negligible R-factor optimization by subsequent TLS refinement strategies. All structures were refined for a total of 5 macrocycles. Statistics for these initial crystal structure models are shown in Supplementary **Table S3** and are available along with the structures at www.rcsb.org in PDB entries 5F66 (CypA) and 5F6M (trypsin).

Supplementary References:

1. Liebschner D, Dauter M, Brzuszkiewicz A, & Dauter Z (2013) On the reproducibility of protein crystal structures: five atomic resolution structures of trypsin. *Acta Crystallogr D Biol Crystallogr* 69(Pt 8):1447-1462.

2. Fraser JS*, et al.* (2009) Hidden alternative structures of proline isomerase essential for catalysis. *Nature* 462(7273):669-673.

3. Kabsch W (2010) Xds. *Acta Crystallogr D Biol Crystallogr* 66(Pt 2):125-132.

4. Winter G, Lobley CM, & Prince SM (2013) Decision making in xia2. *Acta Crystallogr D Biol Crystallogr* 69(Pt 7):1260-1273.

5. McCoy AJ*, et al.* (2007) Phaser crystallographic software. *J Appl Crystallogr* 40(Pt 4):658-674.

6. Adams PD*, et al.* (2010) PHENIX: a comprehensive Python-based system for macromolecular structure solution. *Acta Crystallogr D Biol Crystallogr* 66(Pt 2):213-221.

7. Afonine PV*, et al.* (2012) Towards automated crystallographic structure refinement with phenix.refine. *Acta Crystallogr D Biol Crystallogr* 68(Pt 4):352-367.